Computer Methods in Biomechanics and Biomedical Engineering

Publication details, including instructions for authors and subscription information:
http://www.tandfonline.com/loi/gcmb20

Patient-specific simulation of a stentless aortic valve implant: the impact of fibres on leaflet performance

F. Auricchio [a b c], M. Conti [a], A. Ferrara [a], S. Morganti [a] & A. Reali [a b]

[a] Dipartimento di Ingegneria Civile e Architettura (DICAr), Università degli Studi di Pavia, Via Ferrata 1, 27100, Pavia, Italy

[b] Istituto di Matematica Applicata e Tecnologie Informatiche (IMATI-CNR), Pavia, Italy

[c] Centro di Simulazione Numerica Avanzata (CESNA-IUSS), Pavia, Italy

Available online: 03 May 2012

To cite this article: F. Auricchio, M. Conti, A. Ferrara, S. Morganti & A. Reali (2012): Patient-specific simulation of a stentless aortic valve implant: the impact of fibres on leaflet performance, Computer Methods in Biomechanics and Biomedical Engineering, DOI:10.1080/10255842.2012.681645

To link to this article: http://dx.doi.org/10.1080/10255842.2012.681645

Computer Methods in Biomechanics and Biomedical Engineering
iFirst article, 2012, 1–9

Patient-specific simulation of a stentless aortic valve implant: the impact of fibres on leaflet performance

F. Auricchio[a,b,c], M. Conti[a], A. Ferrara[a], S. Morganti[a]* and A. Reali[a,b]

[a]*Dipartimento di Ingegneria Civile e Architettura (DICAr), Università degli Studi di Pavia, Via Ferrata 1, 27100 Pavia, Italy;* [b]*Istituto di Matematica Applicata e Tecnologie Informatiche (IMATI-CNR), Pavia, Italy;* [c]*Centro di Simulazione Numerica Avanzata (CESNA-IUSS), Pavia, Italy*

(*Received 24 November 2011; final version received 29 March 2012*)

In some cases of aortic valve leaflet disease, the implant of a stentless biological prosthesis represents an excellent option for aortic valve replacement (AVR). In particular, if compared with the implant of mechanical valves, it provides a more physiological haemodynamic performance and a reduced thrombogeneticity, avoiding the use of anticoagulants. The clinical outcomes of AVR are strongly dependent on an appropriate choice of both prosthesis size and replacement technique, which is, at present, strictly related to surgeon's experience and skill. This represents the motivation for patient-specific finite element analysis able to virtually reproduce stentless valve implantation. With the aim of performing reliable patient-specific simulations, we remark that, on the one hand, it is not well established in the literature whether bioprosthetic leaflet tissue is isotropic or anisotropic; on the other hand, it is of fundamental importance to incorporate an accurate material model to realistically predict post-operative performance. Within this framework, using a novel computational methodology to simulate stentless valve implantation, we test the impact of using different material models on both the stress pattern and post-operative coaptation parameters (i.e. coaptation area, length and height). As expected, the simulation results suggest that the material properties of the valve leaflets affect significantly the post-operative prosthesis performance.

Keywords: stentless valve; finite element analysis; patient-specific modelling; fibre-reinforced anisotropic material

1. Introduction

In the last decade, computational tools have been increasingly adopted to investigate biomechanical problems and, in particular, cardiovascular diseases, which are the leading cause of death in the industrialised world (AHA committee 2010). Computational modelling may significantly contribute to move the current paradigm in cardiovascular medicine from 'diagnosis' to 'prediction'. In particular, patient-specific computer-based analyses may be performed to evaluate the efficacy of various possible treatments and to design the optimal intervention, thus representing a useful engineering support during the operation planning procedure (Grande et al. 2000; Soncini et al. 2009; Auricchio et al. 2010).

In this study, we focus our attention on the aortic valve replacement (AVR) technique performed using biological stentless prostheses. Bioprosthetic valves present many advantages as compared with mechanical prostheses: (i) they are associated with minor incidence of haemorrhage, (ii) they avoid the use of anticoagulants and (iii) they result in more physiological haemodynamics (Peterseim et al. 1999; Stassano et al. 2009; Aboud et al. 2010); by contrast, mechanical prostheses assure a long-term solution and should be preferred for young patients (Kulik et al. 2006).

Herein, we propose an engineering procedure based on finite element analysis (FEA), which may give indications on post-operative results after AVR by means of stentless tissue valves. The motivation of our study lies in the technical difficulty of such a surgical operation, which is highly surgeon dependent, and requires an optimal prosthesis sizing specific for each treated patient, which is not a trivial issue. Recent studies have dealt with this problem (Xiong et al. 2010; Auricchio et al. 2011) assuming the leaflet material to be isotropic. In this study, we aim at investigating the effect of the use of a fibre-reinforced model on the prosthesis performance; adopting a correct material model may in fact have a significant influence on the prediction of real valve behaviour.

Bioprosthetic heart valve leaflets are essentially made of glutaraldehyde-treated bovine pericardium. Even though, on the one hand, it is well accepted that the bovine pericardium behaves as an anisotropic material (Radjeman et al. 1985; Yue and Zhong 1988; Zioupos et al. 1992), on the other hand, there are different beliefs concerning the characteristics of the bovine pericardium after the fixation process which was introduced to minimise antigeneticity and maximise biochemical stability of the tissue, preventing in this way autolysis and degradation (Trowbridge and Crofts 1986). Moreover, cross-linking induced by fixation

*Corresponding author. Email: simone.morganti@unipv.it

ISSN 1025-5842 print/ISSN 1476-8259 online

http://dx.doi.org/10.1080/10255842.2012.681645
http://www.tandfonline.com

is strictly dependent on both the methods of fixation, particularly on the initial stress condition (Chachra et al. 1996), and on the mechanical properties of the native, unfixed bovine pericardium.

Langdon et al. (1999) carried out experimental tests on glutaraldehyde-treated bovine pericardium subjected to an equibiaxial load, obtaining stress–strain curves qualitatively showing anisotropy in all testing conditions. Even Arcidiacono et al. (2005), who performed uniaxial tensile tests on 30 glutaraldehyde-fixed bovine pericardial specimens, stated that the tissue presents different mechanical responses depending on the direction of the applied force.

On the contrary, Lee et al. (1989) suggested that, even if fresh pericardial tissue exhibits anisotropy, it may be considered fully isotropic after the fixation process. The same hypothesis has been proposed by Trowbridge et al. (1985), who considered fixed bovine pericardium to be isotropic.

The impact of material modelling on aortic valve performance has been already studied (Koch et al. 2010) and, in particular, the effects of anisotropy on bioprosthetic valve behaviour have been considered in previous studies: Kim et al. (2006), for example, performed dynamic FEA of a biological heart valve prosthesis adopting a generalised nonlinear Fung-type elastic constitutive model.

In this study, after introducing a novel FEA methodology to predict the performance of stentless valves implanted in patient-specific aortic roots, we analyse the impact of the anisotropic model proposed by Holzapfel (Holzapfel et al. 2000), which is well accepted for modelling biological tissues, on both the stress patterns and post-operative coaptation parameters. In particular, the effects of the use of an isotropic hyperelastic material model for the valve leaflets are compared with those of a fibre-reinforced material model taking into account oriented fibre distributions calibrated on experimental curves from tensile tests on glutaraldehyde-treated bovine pericardium (Langdon et al. 1999).

Moreover, we consider the closing phase of the whole valve attached to a patient-specific aortic root, which implies modelling the coaptation between the leaflets including contact.

2. Materials and methods

In this section, we describe how we create the geometrical models and which material constitutive law we adopt. We also present the procedure to reproduce prosthesis implantation and to evaluate post-operative prosthesis competence.

2.1 Geometrical models

Two geometrical models have to be created to simulate the stentless valve implant: (i) the model of the patient-specific aortic root and (ii) the model of the stentless prosthesis.

(i) *Aortic root*. We assume that the recorded diastolic configuration of the aortic root remains the same after the surgical procedure of stentless valve implant. Consequently, the aortic root model adopted for the simulations is obtained from DICOM (Digital Imaging and Communications in Medicine) images of a cardiac computed tomography-angiography (CT-A) performed using an iodinate contrast die on a 46-year-old male patient. The CT-A scan has been performed at IRCCS Policlinico San Matteo, Pavia, Italy, using a SOMATOM Sensation Dual Energy scanner (Siemens Medical Solutions, Forchheim, Germany). The scan data are characterised by the following features: slice thickness: 0.6 mm; slice width × height: 512 × 512; pixel spacing: 0.56 mm. The stereolithographic (STL) description of the aortic root is achieved using ITK-SNAP v2.0.0 (Yushkevich et al. 2006). Then, the obtained STL representation is processed in Matlab (Natick, Massachusetts, USA) to generate the CAD model of the aortic root under investigation, which is then meshed within the finite element solver Abaqus (v6.10, Simulia, Dassáult Systems, Providence, RI, USA) with 11410 linear triangular shell elements (S3R). In Figure 1, the main steps to obtain a finite element mesh of a patient-specific aortic root are highlighted.

(ii) *Stentless valve*. The stentless valve geometry is based on the simplified Labrosse model (Labrosse et al. 2006), which is completely described by the following five parameters as highlighted in Figure 2:

Figure 1. Aortic root model: DICOM files of CT-A images are processed to get the STL description of the aortic root. This is converted into a CAD model and, then, a triangular shell element mesh is constructed.

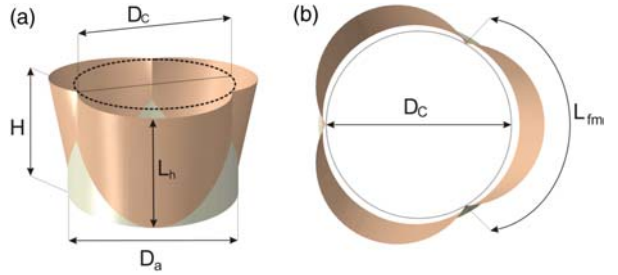

Figure 2. Labrosse geometric model of a healthy valve: (a) the perspective view shows parameters D_a, D_c, H and L_h; (b) the top view highlights L_{fm} and, again, D_c. Reprinted from Auricchio et al. (2011), with permission from Elsevier.

- the diameter of the annulus, D_a;
- the diameter of the top of the commissure, D_c;
- the valve height, H;
- the leaflet free margin length, L_{fm};
- the leaflet height, L_h.

No technical data has been received by the manufacturer. For this reason, the Labrosse valve parameters are defined on the basis of the Freedom Solo valve (Sorin Biomedica Cardio, Saluggia, Italy) basic dimensions, highlighted in Figure 3 and reported in the product catalogue. In order to obtain the whole set of needed dimensions, we assume that the prosthetic tissue valve has the same geometrical features of a healthy human aortic valve (Aymard et al. 2010). The adopted parameter values are $D_a = 27$ mm, $D_c = 25$ mm, $H = 18$ mm, $L_{fm} = 33$ mm and $L_h = 18$ mm.

The leaflets are meshed within Abaqus using 11242 triangular membrane elements (M3D3).

2.2 Materials

(i) *Aortic root*. Since in this study we mainly focus on the study of aortic valve leaflets, we use a simplified material model for the aortic root. In particular, following Ranga et al. (2007), we adopt an incompressible isotropic hyperelastic Mooney–Rivlin model, defined by the following strain energy potential (Yeoh 1993):

$$\Psi = c_{10}(I_1 - 3) + c_{01}(I_2 - 3), \quad (1)$$

where c_{10} and c_{01} are the material parameters whereas I_1 and I_2 are the first and second invariant of the right Cauchy-Green deformation tensor $\mathbf{C}$:

$$I_1 = \operatorname{tr}\mathbf{C}, \quad I_2 = \frac{1}{2}\left[I_1^2 - \operatorname{tr}\mathbf{C}^2\right]. \quad (2)$$

As proposed by Einstein et al. (2003), we adopt the following parameter values: $c_{10} = 0.5516$ MPa and $c_{01} = 0.1379$ MPa. The density is set to 1000 kg/m^3.

(ii) *Stentless valve*. Microscopic examination of bovine pericardium specimens reveals the structural organisation of the tissue, which appears as a fibrous network containing mainly elastin and collagen fibres saturated with a high water content (Sanchez-Arevalo et al. 2010). In this study, for the valve leaflets, we consider two different material models in order to evaluate the influence of the considered constitutive law on the performance of the replacement technique.

In the first case (material A), we consider a simple isotropic nearly incompressible hyperelastic material exploiting a linear relationship between the Cauchy stress and the logarithmic strain measures and, in particular, characterised by a Young modulus of 8 MPa, a Poisson ratio of 0.49 and a density of 1100 kg/m^3: such values are within the statistical range of the treated pericardial tissue (Zioupos et al. 1994; Xiong et al. 2010).

In the second case (material B), we model the leaflets using the anisotropic model proposed by Holzapfel (2000), which takes into account the collagen fibre orientation. According to the considered model, the strain energy function is defined as follows:

$$\Psi = c_{10}(I_1 - 3) + \sum_i \frac{k_{1i}}{2k_{2i}}\{\exp[k_{2i}(I_{4i} - 1)^2] - 1\}, \quad (3)$$

where $c_{10} \geq 0$ is related to the mechanical response of the non-collagenous matrix, whereas the parameters $k_{1i} > 0$ and $k_{2i} > 0$ are associated with the response of the ith collagen fibre. It is worth noting that the invariant I_{4i} is the square of the stretch along the ith preferred direction identified by the unit vector $\mathbf{a}_{0i}$. In particular,

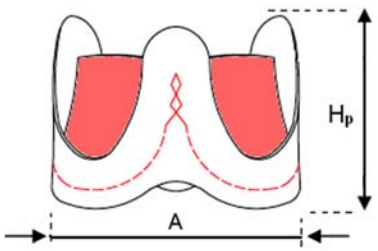

REF	ART. 23 SG	ART. 25 SG	ART. 27 SG
Ord.code	ICVD902	ICVD903	ICVD904
A [mm]	25	27	29
Hp [mm]	21	22	23

Figure 3. Freedom SOLO main dimensions as reported in the product catalogue.

it is defined as

$$I_{4i} = \mathbf{C} : \mathbf{a}_{0i} \otimes \mathbf{a}_{0i}. \tag{4}$$

As discussed in Sacks et al. (1994), it is acceptable to consider two families of fibres for the bovine pericardium symmetrically organised with respect to the base-to-apex direction (see Figure 4(a)). Assuming a local base $\{\mathbf{e}_1,\mathbf{e}_2,\mathbf{e}_3\}$ with $\mathbf{e}_1$ oriented along the base-to-apex direction, $\mathbf{e}_2$ orthogonal to $\mathbf{e}_1$ lying in the plane of the pericardium sheet and $\mathbf{e}_3 = \mathbf{e}_1 \wedge \mathbf{e}_2$, the unit vectors $\mathbf{a}_{01}$ and $\mathbf{a}_{02}$ have the following components:

$$\begin{aligned} \mathbf{a}_{01} &= \cos\beta\,\mathbf{e}_1 + \sin\beta\,\mathbf{e}_2 + 0\mathbf{e}_3, \\ \mathbf{a}_{02} &= \cos\beta\,\mathbf{e}_1 - \sin\beta\,\mathbf{e}_2 + 0\mathbf{e}_3, \end{aligned} \tag{5}$$

with $\pm\beta$ being the constant angles between the base-to-apex direction and the vectors $\mathbf{a}_{01}$ and $\mathbf{a}_{02}$, respectively.

In agreement with experimental evidences, the fibres are predominantly aligned along the base-to-apex direction, making this the least extensible direction.

When modelling valve leaflets, we assume that the unit vector $\mathbf{e}_1$ is oriented along the circumferential direction, since it is known that valve leaflets are much stiffer (i.e. collagen fibres are preferentially oriented) in the circumferential direction (Billiar and Sacks 2000; Driessen et al. 2005) as shown in Figure 4(b).

Assuming that the two fibre families are mechanically equivalent, we have $k_{11} = k_{12} = k_1$ and $k_{21} = k_{22} = k_2$. As no information on the collagen fibre orientation is available for the investigated material, we also assume the angle β defining such an orientation to be an unknown parameter. It follows that the model of Equation (3) is characterised by four independent parameters, i.e. c_{10}, k_1, k_2 and β.

The material parameters are extracted from the biaxial tests on glutaraldehyde-fixed bovine pericardium tissue carried out by Langdon et al. (1999) using a nonlinear least square method. Such an optimisation technique requires the identification of both the experimental stress data $\sigma^{\exp}$ and the related theoretical values σ^{mod}.

The experimental data $\sigma^{\exp}$ are obtained from Langdon et al. (1999) in which the material response is reported in terms of Cauchy stress versus engineering strain. On the other hand, the Cauchy stresses predicted by the strain energy function Ψ are given by

$$\sigma_{11}^{\mathrm{mod}} = \frac{\partial\Psi}{\partial\lambda_1}\cdot\lambda_1, \quad \sigma_{22}^{\mathrm{mod}} = \frac{\partial\Psi}{\partial\lambda_2}\cdot\lambda_2, \quad \sigma_{33}^{\mathrm{mod}} = 0, \tag{6}$$

where λ_1 and λ_2 are the stretches in the directions $\mathbf{e}_1$ and $\mathbf{e}_2$, respectively.

Then, the optimisation problem consists of minimising the objective function χ^2 defined as the squared sum of the differences between the experimental data and the related model prediction variable:

$$\chi^2 = \sum_{a=1}^{p} \left[\left(\sigma_{11,a}^{\mathrm{mod}} - \sigma_{11,a}^{\exp}\right)^2 + \left(\sigma_{22,a}^{\mathrm{mod}} - \sigma_{22,a}^{\exp}\right)^2 \right], \tag{7}$$

where p represents the number of data points.

In our computations, we do not impose particular upper and lower bounds on the material parameters except those necessary to define the domain of the considered strain energy functions, thus discarding non-physical solutions. Since the convergence of the algorithm depends on the initial guess, we repeat the optimisation procedure for a wide range of initial parameters checking that the algorithm convergence to the optimal sets is not affected by the start guess and by the numerical accuracy required by the algorithm.

From the best fitting procedure, the coefficient c_{10} results equal to 0. Since the use of null values of c_{10} leads to unstable, non-physiological phenomena during the numerical simulations, we force such a parameter to

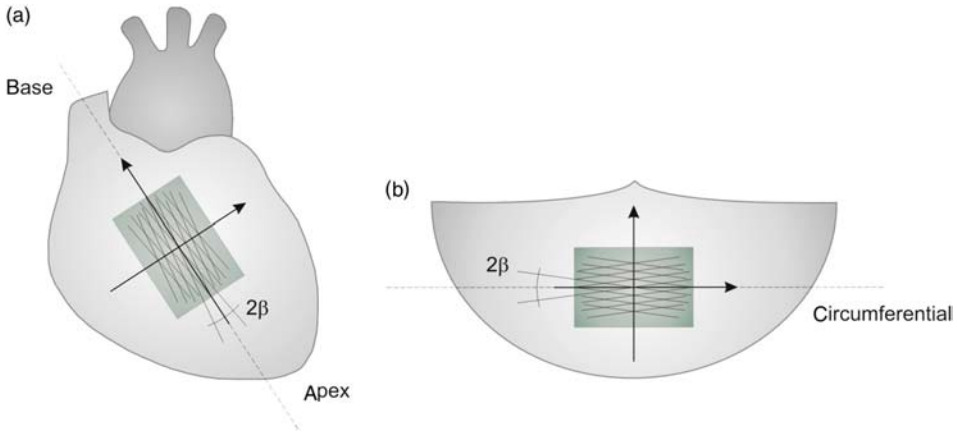

Figure 4. Orientation of the two families of fibres: (a) in the bovine pericardium; (b) in the valve leaflet.

assume non-null values. The introduced expedient implies a non-optimal correspondence between experimental data and fitted values for low stretches.

The trade-off between an accurate result from the fitting procedure and a numerically stable solution of the FEAs, which respects the physiological behaviour, leads to the estimated parameter values $c_{10} = 20.1$ kPa, $k_1 = 54.62$ kPa, $k_2 = 30.86$ and $\beta = 29.8°$. The associated curve fitting is shown in Figure 5.

2.3 Prosthesis placement simulation

As highlighted in Figure 6, the prosthesis implant is simulated by constraining the attachment lines of the leaflet (red lines in the figure) to overlap the so-called 'suture-lines', properly defined on the patient-specific aortic root model (blue lines in the figure).

A quasi-static FEA of the prosthesis placement is performed using the Abaqus Explicit solver; pre-computed displacements are imposed to the nodes of the prosthesis attachment lines. Inertia forces do not dominate the analysis, as proven by the ratio of kinetic to internal energy which remains below 5%.

2.4 Prosthesis closure simulation

To evaluate the performance of the implanted prosthetic valve, we simulate the diastolic phase of the cardiac cycle. The CT-A data adopted to generate the geometrical model of the aortic root wall have been obtained at the end of the diastolic phase; for this reason, a uniform pressure $p = 80$ mmHg is gradually applied to the leaflets, while the pressure acting on the internal wall of the sinuses is kept equal to zero. The nodes belonging both to the top and

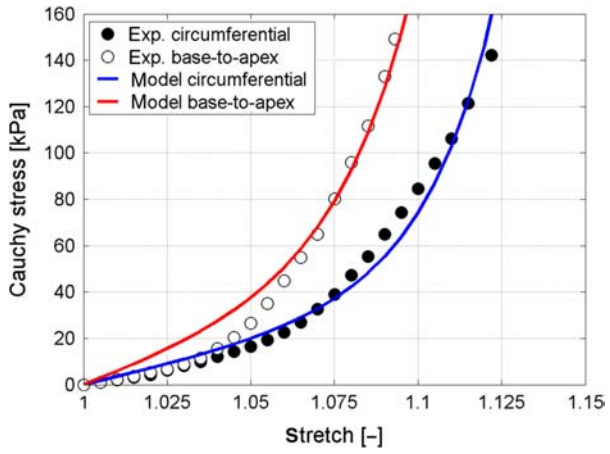

Figure 5. Circumferential and base-to-apex stress–stretch response of bovine pericardium (Langdon et al. 1999) compared with numerical results obtained by using the model proposed by Holzapfel et al. (2000).

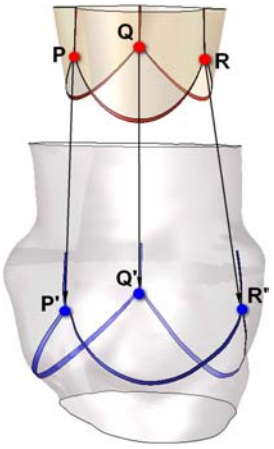

Figure 6. Simulation strategy for the prosthesis placement: the black arrows represent the displacements to be computed and applied to the nodes of the prosthesis attachment lines. Reprinted from Auricchio et al. (2011), with permission from Elsevier.

to the bottom of the aortic root model are confined to the plane of their original configuration.

In Figure 7, a representative sketch of the boundary conditions applied to simulate valve closure is depicted.

The numerical analysis of the prosthesis closure consists of a highly nonlinear problem involving large deformations and contact. For this reason, the Abaqus Explicit solver is used to perform the simulations; in particular, quasi-static procedures are used again, assuming that inertia forces do not affect the solution. Kinetic energy is monitored to ensure that the ratio of kinetic to internal energy remains below 10%.

To study the stress distribution on the leaflets, in order to neglect peak values that can be affected by local effects, we consider only the 99 percentile with respect to the original leaflet area (i.e. we neglect the 1% of the area characterised by the highest stress values) and we compute

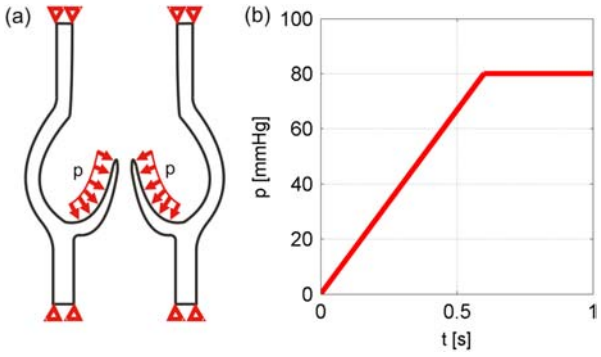

Figure 7. Simulation of prosthesis closure: (a) sketch of the applied boundary conditions; (b) pressure on the leaflets as a function of time. Reprinted from Auricchio et al. (2011), with permission from Elsevier.

the average stress, σ_{av}, as

$$\sigma_{av} = \frac{\sum_{i=1}^{N} \sigma_i A_i}{\sum_{i=1}^{N} A_i}, \quad (8)$$

where σ_i is the stress evaluated at the centre of each element, A_i is the element area and N is the number of considered elements.

3. Results

FEA is first performed to reproduce the implant of the aortic valve prosthesis and, then, once the prosthesis is virtually implanted and sutured inside the aortic root, a uniform pressure is applied to the leaflets in order to evaluate the performance of the reproduced surgical solution with particular focus on the effect of the chosen material model.

First of all, it is possible to observe that the adopted anisotropic material model produces reduced stress values on the leaflets with respect to the isotropic material model. Just comparing the maximum von Mises stress values, we have: $\sigma_M^A = 3.85\,\text{MPa}$ and $\sigma_M^B = 3.42\,\text{MPa}$, where the superscripts A and B stand for 'material A' and 'material B', respectively.

In Figure 8, the von Mises stress patterns are represented for each investigated case using the same colour scale. The obtained values of σ_{av} are $\sigma_{av}^A = 0.21\,\text{MPa}$ and $\sigma_{av}^B = 0.14\,\text{MPa}$. In Figure 9, the vector plot of the maximum principal stress is shown from a top view. In the anisotropic case (Figure 9(b)), the stresses are predominantly aligned along the circumferential direction rather than in the isotropic case where the stresses are slightly more uniformly distributed.

Measures of coaptation are other important outcomes of our simulations, since they explicitly indicate whether the simulated surgical intervention fails or not. In particular, we are able to measure (see Figure 10) (i) the coaptation length, L_c, defined as the maximum effective length of coaptation; (ii) the height of coaptation, H_c, which is the distance between the plane in which the annulus lies and the point in which coaptation occurs and (iii) the coaptation area, A_c, defined as the total area of the elements in contact.

In Table 1, the measured values are summarised highlighting significant differences between an isotropic valve behaviour and an anisotropic valve behaviour.

4. Discussion and conclusion

In this study, we propose a novel approach to investigate by means of computational tools the implant of biological stentless valves. Through patient-specific FEA we are able to virtually reproduce the post-operative behaviour of a stentless valve, which means identifying the potential optimal surgical solution better tailored to the specific patient. Once the procedure has been developed, in fact, it is possible to investigate the impact of different factors (e.g. prosthesis type, prosthesis size and suture-line position) on the valve performance. In particular, this study aims at evaluating the influence of the adopted material model for the valve leaflets.

In the literature, several studies on the bovine pericardium are reported (Lee and Boughner 1981; Wiegner et al. 1981; Yin et al. 1986; Zioupos et al. 1992).

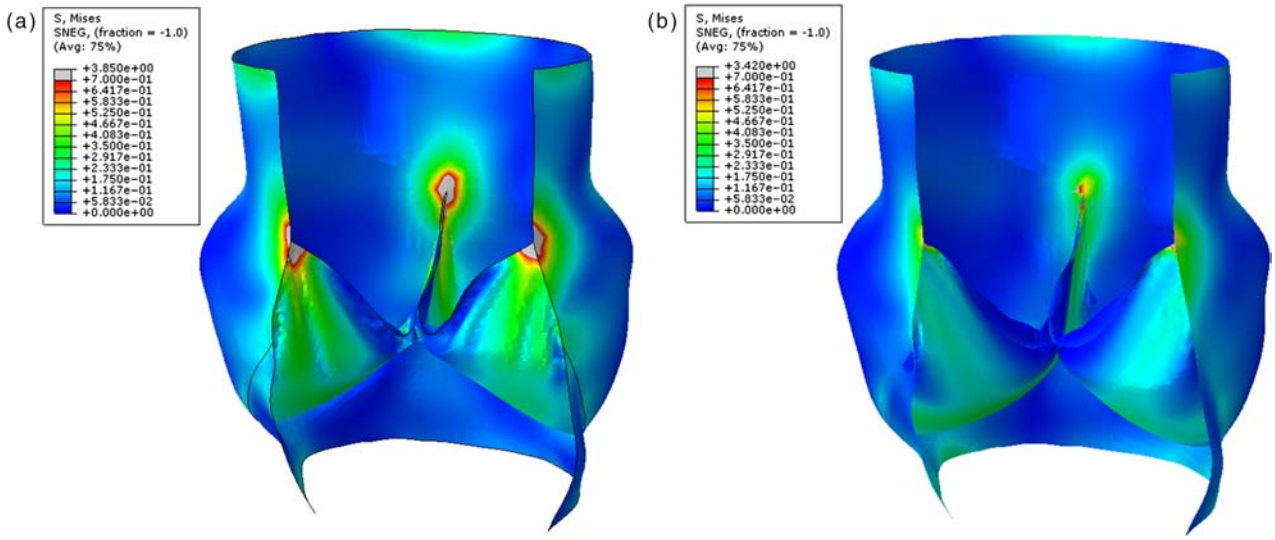

Figure 8. von Mises stress pattern at the end of diastole: (a) isotropic material model; (b) fibre-reinforced model. A cut view is adopted to highlight the coaptation.

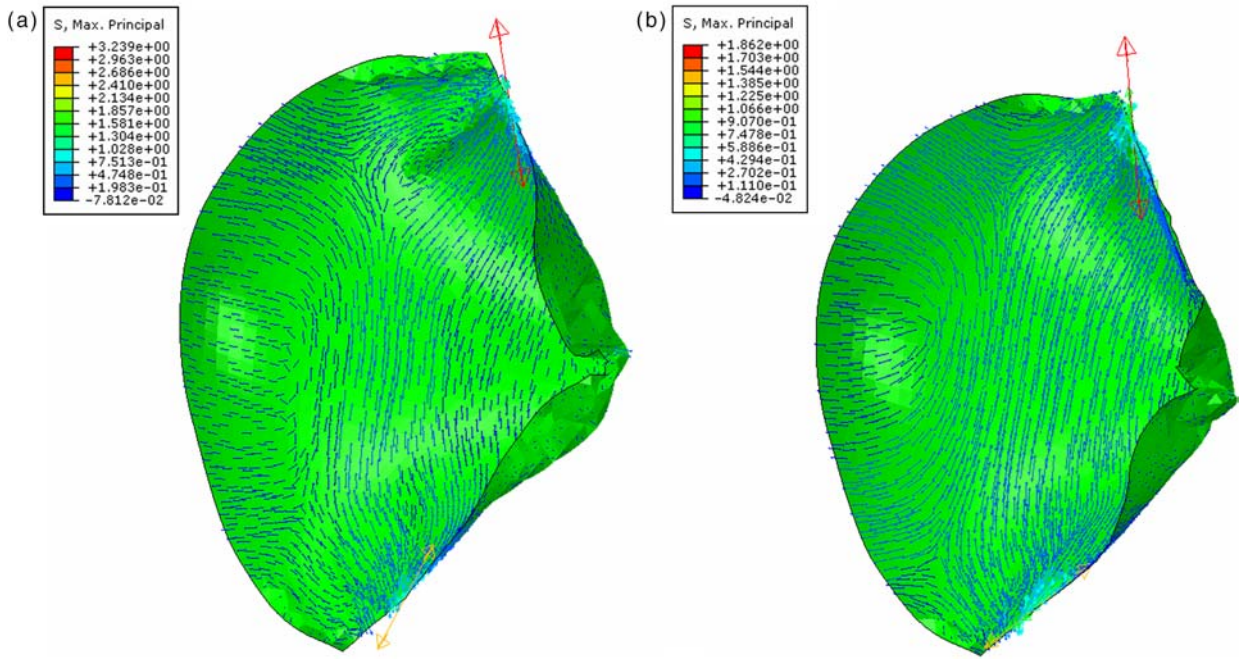

Figure 9. Vector plot of the maximum principal stress of the closed leaflets at the end of diastole: (a) isotropic material model; (b) anisotropic Holzapfel material model. The bigger arrows close to the commissures show a stress concentration in that region.

It is well accepted that the bovine pericardium is an anisotropic material; however, there is no univocal opinion on the glutaraldehyde-treated pericardium: according to some authors, in fact, the chemical fixation process makes it behave like an isotropic material (Trowbridge et al. 1985; Lee et al. 1989), while others claim that it maintains its original anisotropic characteristics even after the fixation procedure (Langdon et al. 1999; Arcidiacono et al. 2005). For this reason, in this study we analyse the differences of considering an isotropic or a fibre-reinforced anisotropic model for the valve leaflets.

First of all, we may observe that the maximum principal stress distribution on the closed valve leaflets is more uniformly aligned in case of anisotropic material model (see Figure 9(b)) with respect to an isotropic model (see Figure 9(a)). We may conclude that the fibres drive the stress distribution predominantly in the direction of their alignment (i.e. circumferentially). This aspect also leads to the reduced stress values obtained adopting an anisotropic material model with respect to an isotropic model. This is in agreement with results presented in previous studies (Koch et al. 2010).

Moreover, the performed simulations confirm that anisotropic leaflets have a significantly greater coaptive area as reported in Table 1 and exhibit a smoother closure. It is observed that at the end of diastole, the isotropic leaflets (Figure 9(a)) exhibit many non-physiological foldings and wrinkles, particularly close to the commissures, which are not present in the closed configuration of the anisotropic leaflets (Figure 9(b)).

Furthermore, the coaptation length increases while the coaptation height decreases when moving from an isotropic to an anisotropic model. Even such a result is in agreement with previously published studies (Koch et al. 2010), confirming that the introduction of anisotropy in the leaflet model leads to both an increased compliance in the radial direction and an improved coaptation. Based on the results of our study, we conclude that the choice of material model significantly influences the performance of the implanted valve and, therefore, it represents a crucial issue when performing numerical simulations.

In dealing with the limitations of the present study, to achieve a more realistic representation of reality, an anisotropic model for the aortic root accounting for the

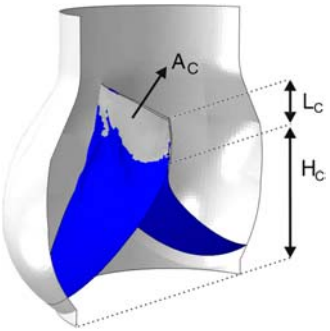

Figure 10. Illustrative representation of the measured coaptation parameters: area of coaptation, A_c; coaptation length, L_c and coaptation height, H_c.

Table 1. Length L_c, height H_c and area A_c of coaptation obtained from each simulation.

Mat ID	L_c (mm)	H_c (mm)	A_c (mm^2)
A	2.75	16.8	277.5
B	7.57	13.03	609.4

pre-stress should be considered. Moreover, modelling the fluid-structure interaction between the valve leaflets and blood could give useful additional information. These improvements are currently under investigation and will be the subject of future communications. Finally, if, on the one hand, the aortic root model is a true representation of the patient's aortic root, on the other hand, the prosthesis model is just an approximation of the real prosthesis available on the market. The creation of models completely based on product specification data, unfortunately currently unavailable, would improve the outcome of the simulations; this certainly represents a future development of this study. However, the geometrical modelling of the stentless valve as a healthy human valve is commonly accepted (see, e.g. Aymard et al. (2010)).

Acknowledgements

The authors have been partially supported by the Cariplo Foundation through the Project no. 2009.2822 and by the European Research Council through the Project no. 259229 entitled 'ISOBIO: Isogeometric Methods for Biomechanics'. The authors would like to acknowledge Dott. Totaro of IRCCS Policlinico San Matteo, Pavia, Italy, for providing useful clinical comments on the procedure of stentless valve implant, Dott. R. Dore of IRCCS Policlinico San Matteo, Pavia, Italy, for support to the medical and imaging aspects of the present work and Eng. Carolina Ferrazzano, Structural Mechanics Department, University of Pavia, Italy, for her support in medical image processing.

References

Aboud A, Breuer M, Bossert T, Gummert JF. 2010. Quality of life after mechanical vs. biological aortic valve replacement. Asian Cardiovasc Thorac Ann. 17:35–38.

AHA committee. 2010. Heart disease and stroke statistics 2010 update: a report from the American heart association. Circulation. 121:e46–e215.

Arcidiacono G, Corvi A, Severi T. 2005. Functional analysis of bioprosthetic heart valves. J Biomech. 38:1483–1490.

Auricchio F, Conti M, Demertzis S, Morganti S. 2010. Finite element analysis of aortic root dilation: a new procedure to reproduce pathology based on experimental data. Comput Methods Biomech Biomed Engin. 14(10):875–882, DOI:10.1080/10255842.2010.499867.

Auricchio F, Conti M, Morganti S, Totaro P. 2011. A computational tool to support pre-operative planning of stentless aortic valve prosthesis. Med Eng Phys. 33(10):1183–1192, DOI:10.1016/j.medengphy.2011.05.006.

Aymard T, Eckstein F, Englberger L, Stalder M, Kadner A, Carrel T. 2010. The Sorin Freedom SOLO stentless aortic valve: technique of implantation and operative results in 109 patients. J Thorac Cardiovasc Surg. 139:775–777.

Billiar KL, Sacks MS. 2000. Biaxial mechanical properties of the natural and glutaraldehyde treated aortic valve cusp-part I: experimental results. J Biomech Eng. 122:23–30.

Chachra D, Gratzer PF, Pereira CA, Lee JM. 1996. Effect of applied uniaxial stress on rate and mechanical effects of cross-linking in tissue-derived biomaterials. Biomaterials. 17:1865–1875.

Driessen NJB, Bouten CV, Baaijens FP. 2005. A structural constitutive model for collagenous cardiovascular tissues incorporating the angular fiber distribution. J Biomech Eng. 127:494–503.

Einstein DR, Reinhall P, Nicosia M, Cochran RP, Kunzelman KS. 2003. Dynamic finite element implementation of nonlinear, anisotropic hyperelastic biological membranes. Comput Methods Biomech Biomed Engin. 6:33–44.

Grande KJ, Cochran RP, Reinhall PG, Kunzelman KS. 2000. Re-creation of sinuses is important for sparing the aortic valve: a finite element study. J Thorac Cardiovasc Surg. 119:753–763.

Holzapfel GA, Gasser TC, Ogden RW. 2000. A new constitutive framework for arterial wall mechanics and a comparative study of material models. J Elasticity. 61:1–48.

Kim H, Lu J, Sacks MS, Chandran KB. 2006. Dynamic simulation pericardial bioprosthetic heart valve function. J Biomech Eng. 128:717–724.

Koch TM, Reddy BD, Zilla P, Franz T. 2010. Aortic valve leaflet mechanical properties facilitate diastolic valve function. Comput Methods Biomech Biomed Engin. 13(2):225–234.

Kulik A, Bedard P, Lam B-K, Rubens FD, Hendry PJ, Masters RG, Mesana TG, Ruel M. 2006. Mechanical versus bioprosthetic valve replacement in middle-aged patients. Eur J Cardiothorac Surg. 30:485–491.

Labrosse MR, Beller CJ, Robicsek F, Thubrikar MJ. 2006. Geometric modeling of functional trileaflet aortic valves: development and clinical applications. J Biomech. 39:2665–2672.

Langdon SE, Chernecky R, Pereira CA, Abdulla D, Lee JM. 1999. Biaxial mechanica/structural effects of equibiaxial strain during crosslinking of bovine pericardial xenogrfat materials. Biomaterials. 20:137–153.

Lee J, Boughner DR. 1981. Tissue mechanics of canine pericardium in different test environments. Circ Res. 49:533–544.

Lee J, Haberer SA, Boughner DR. 1989. The bovine pericardial xenograft: I. Effects of fixation in aldehydes without constraints on the tensile viscoelastic properties of bovine pericardium. J Biomed Mater Res. 23:457–475.

Peterseim DS, Cen Y-Y, Cheruvu S, Landolfo K, Bashore TM, Lowe JE, Wolfe WG, Glower DD. 1999. Long-term outcome after biologic versus mechanical aortic valve replacement in 841 patients. J Thorac Cardiovasc Surg. 117:890–897.

Radjeman A, Liew SC, Lim KO. 1985. Anisotropic elasicity of bovine pericardial tissue. Jpn J Physiol. 35:831–840.

Ranga A, Mongrain R, Biadilah Y, Cartier R. 2007. A compliant dynamic FEA model of the aortic valves. In: Proceedings of 12th IFToMM World Congress. Besancon.

Sacks MS, Chuong CJ, More R. 1994. Collagen fiber architecture of bovine pericardium. ASAIO J. 40:M632–M637.

Sanchez-Arevalo FM, Farfan M, Covarrubias D, Zenit R, Pulos G. 2010. The micromechanical behavior of lyophilized glutaraldehyde-treated bovine pericardium under uniaxial tension. J Mech Behav Biomed Mater. 3:640–646.

Soncini M, Votta E, Zinicchino S, Burrone V, Mangini A, Lemma M, Antona C, Redaelli A. 2009. Aortic root

performance after valve sparing procedure: a comparative finite element analysis. Med Eng Phys. 31:234–243.

Stassano P, DiTommaso L, Monaco M, Iorio F, Pepino P, Spampinato N, Vosa C. 2009. Aortic valve replacement: a prospective randomized evaluation of mechanical versus biological valves in patients ages 55 to 70 years. J Am Coll Cardiol. 54:1862–1868.

Trowbridge EA, Black MM, Daniel CL. 1985. The mechanical response of glutaraldehyde fixed bovine pericardium to uniaxial load. J Mater Sci. 20:114–140.

Trowbridge EA, Crofts CE. 1986. The extension rate inependence of the hysteresis in glutaraldehyde-fixed bovine pericardium. Biomaterials. 8:201–206.

Wiegner AW, Bing OHL, Borg TK, Cauldfield JB. 1981. Mechanical and structural correlates of canine pericardium. Circ Res. 49:807–814.

Xiong FL, Goetz WA, Chong CK, Chua YL, Pfeifer S, Wintermantel E, Yeo JH. 2010. Finite element investigation of stentless pericardial aortic valves: relevance of leaflet geometry. Ann Biomed Eng. 38:1908–1918.

Yeoh OH. 1993. Some forms of the strain energy function for rubber. Rubber Chem Technol. 66:754–771.

Yin FCP, Chew PH, Zeger SL. 1986. An approach to quantification of biaxial tissue stress–strain data. J Biomech. 19:27–37.

Yue YL, Zhong SP. 1988. The mechanical anisotropy of the Yak pericardium. 3rd World Biomaterials Congress, Kyoto, Japan, p. 77.

Yushkevich PA, Piven J, Hazlett HC, Smith RG, Ho S, Gee JC, Gerig G. 2006. User-guided 3D active contour segmentation of anatomical structures: significantly improved efficiency and reliability. Neuroimage. 31:1116–1128.

Zioupos P, Barbenel JC, Fisher J. 1992. Mechanical and optical anisotropy of bovine pericardium. Med Biol Eng Comput. 30:76–82.

Zioupos P, Barbenel JC, Fisher J. 1994. Anisotropic elasticity and strength of glutaraldehyde fixed bovine pericardium for use in pericardial bioprosthetic valves. J Biomed Mater Res. 28:49–57.